Performance Scaling of mmWave Personal IoT Networks (PINs) for XR Applications

Asad Ali[1,2], Olga Galinina[1,3], Jiri Hosek[2], and Sergey Andreev[1]
[1]Tampere University, Tampere, Finland
[2]Brno University of Technology, Brno, Czech Republic
[3]Institute for Advanced Study, Tampere University, Tampere, Finland
{asad.ali, olga.galinina, sergey.andreev}@tuni.fi, hosek@vut.cz

***Abstract*—To provide a high-quality user experience in Extended Reality (XR) applications, high-throughput and low-latency communication is essential. A promising solution is the use of distributed networks operating in the higher frequency bands, such as millimeter-wave (mmWave) wearable Personal IoT Networks (PINs). However, in crowded environments, intra-network interactions can disrupt the Quality of Experience (QoE) for users. To improve the QoE, the understanding of the system-level performance trade-offs in these networks is important. This paper investigates the impact of various system parameters on the system-level performance of mmWave wearable PINs with 3D beamforming and data rate adaptation to the channel conditions in an environment with human body blockage. We employ an analytical methodology that combines stochastic geometry and queueing theory to devise an expression for the stationary distribution of the system and use it to compute the key metrics that describe the system-level performance. To assess mmWave PINs for XR in crowded environments, we examine the system operation trade-offs and explore the performance scaling.**

***Index Terms*—Wearable Personal IoT Networks, millimeter-wave communication, spatial sharing, elastic traffic, stochastic geometry, queueing theory.**

I. Introduction

Forthcoming high-end wearables such as Extended Reality (XR) headsets (i.e., Augmented Reality (AR) glasses and Mixed Reality (MR) goggles) for immersive applications are expected to have a form-factor and weight similar to regular eyeglasses, which results in hardware constraints such as limited processing power, memory, and battery capacity. XR headsets also impose stringent wireless connectivity requirements, including high reliability, extremely high data rates, and low latency, all stemming from the nature of human visual perception. To meet these requirements, XR headsets may tap into the millimeter-wave (mmWave) frequency band.

Additionally, XR headsets may offload certain tasks to more capable personal devices, such as smartphones or tablets, by tethering via a mmWave link [1], [2], thereby effectively forming a wearable Personal IoT Network (PIN). Wearable PIN refers to a personal network of wearable devices connected via direct radio links in close proximity to a user. The direct connection may include 3GPP and non-3GPP access in licensed or unlicensed spectrum. In this setup, user personal devices can process power-intensive tasks and also act as a relay by providing IP connectivity.

An example XR application that could benefit from this setup is the metaverse, which has the potential to significantly impact the ways we interact with digital content and each other in the future. The 3GPP is currently working on defining the requirements and specifications for Localized Mobile Metaverse Services (LMMS) [3] to facilitate user access to virtual worlds and metaverses with high-quality graphics and real-time interactions in a specific geographic area. Here, XR applications can rely on split-rendering mechanisms, where the XR headset requests the personal device to render frames [4]. However, in dense environments, PINs are exposed to interference from neighboring networks, which can cause a sharp deterioration in throughput and reliability.

Prior research on mmWave PINs has primarily focused on static systems to address the spatial aspects of network interactions and assume full-buffer traffic. For example, studies in [5], [6] employed stochastic geometry to analyze the system-level performance of mmWave PINs equipped with directional antennas and evaluate the impact of interference. The work in [7] proposed a joint PHY-MAC approach to achieve higher data rates and improve the coexistence between different networks. Similarly, the work in [8] utilized stochastic geometry to assess the interference and performance of mmWave wearable networks in high-density settings. However, these studies are limited to the spatial aspect of network interactions and do not fully consider the temporal dimension of system operation. Capturing the PIN's temporal interactions in addition to its spatial characteristics is crucial for a comprehensive evaluation of the system performance.

To address this limitation, individual works have attempted to capture both temporal and spatial characteristics of different types of networks by applying stochastic geometry and queueing theory. For instance, in [9], the session-level service dynamics of user equipment (UE) capable of operating in both microwave and mmWave bands were studied. Similarly, stochastic geometry and queueing theory have been used to investigate the end-to-end delay for XR services that offload traffic to the network infrastructure over THz links [10]. While these models capture the spatio-temporal impact of traffic on network performance, dynamic interactions between distributed networks with directional communication have not been fully explored. Consequently, in our previous study [11], we examined the system-level performance of mmWave PINs

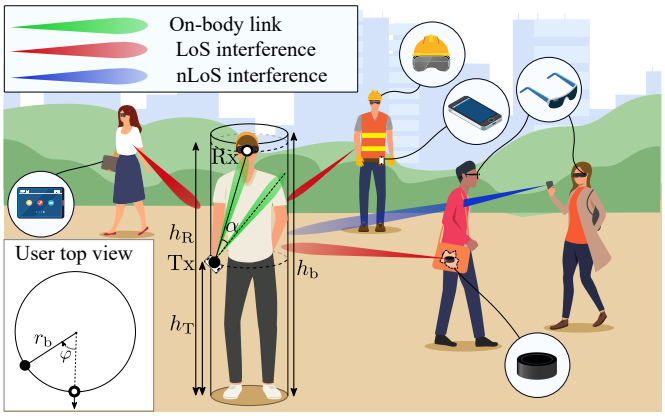

Fig. 1: Motivating scenario: deployment of wearable PINs.

using CSMA/CA channel access without taking into account the impact of human body blockage in the channel. Moreover, the channel was assumed to be occupied exclusively by a single user for the duration of its session, and in the event of contention, other users were denied access to the channel.

To the best of our knowledge, there is no prior research that has utilized a joint stochastic geometry and queuing theory modeling approach to evaluate the performance of mmWave PINs where the channel resources may be shared among the coexisting networks. To bridge that gap, in this study, we investigate the impact of 3D directional communication in a system of PINs operating in the mmWave band. In this system, the data rate on a link adapts according to the channel conditions in an environment with human body blockage. The main contributions of this study are twofold:

- We apply a spatio-temporal modeling approach to offer an analytical methodology for evaluating distributed mmWave XR networks with dynamic data rates in a 3D setup with directional beams and blockers.
- We analyze the system-level performance of mmWave PINs for various system parameters and provide insights into the system-level performance trade-offs and scaling.

The remainder is structured as follows. Section II provides an overview of our system model and its corresponding assumptions. Section III outlines the proposed analytical framework, 3D modeling, and approximation techniques used to derive the relevant metrics. Section IV presents the selected numerical results, and the conclusions are offered in Section V.

II. System Model

This section outlines our system model and its underlying assumptions. We start by presenting our network deployment, then examine the traffic-related considerations for data transmission and the antenna abstraction, and finally provide details on the radio-specific assumptions.

1) Network Deployment: We consider an area of size S_R in $\mathcal{R}^2$, with a total number of M users distributed uniformly within this area of interest. Each user is associated with a wearable PIN, which includes a personal device (Tx) and an XR headset (Rx), as shown in Fig. 1. Every user is modeled as a cylinder with a fixed height h_b and an internal radius r_b. The Tx and Rx are assumed to be located on the associated user at fixed heights h_{tx} and h_{rx}, respectively. The 2D position of the Rx is determined using the front-facing direction of the user. The front-facing direction is selected randomly and uniformly within $[0, 2\pi)$, and it also determines the 2D position of the Tx. The Tx device is placed on the surface of the cylinder at a fixed central angle φ from the Rx, where $\varphi \in [0, \frac{\pi}{2}]$. The resulting constant distance between the paired devices is given by:

$$d = \sqrt{(2r_b \sin \tfrac{\varphi}{2})^2 + (h_{\text{tx}} - h_{\text{rx}})^2}. \tag{1}$$

2) Traffic Model: In this study, we primarily focus on the downlink data transmission (from the Tx to the Rx), since in immersive XR applications, the XR headset primarily receives rendered data [12]. We refer to this data as a file and model the arrivals of file transmission requests as a Poisson process with rate λ_R for each user (i.e., requests per second per user). The size of the files to be transmitted is distributed exponentially with an average of s bits.

3) Antenna Model: The transmission beams are directional in 3D space, all having an axially symmetric main lobe and no side lobes due to tapering. The main lobe is defined by the parameter θ, which denotes the half-power beamwidth (HPBW). The antenna directivity gain is approximated by the product of two components: the maximum directivity factor $G_{\max} = \frac{2}{1-\cos\frac{\theta}{2}}$ and the gain reduction factor $\rho(\alpha)$ defined by the deviation angle α from the antenna boresight, i.e., $G_{\text{tx}} = G_{\max}\rho(\alpha)$. The reduction factor $\rho(\alpha)$ determines the pattern of the antenna radiation in 3D space. For an HPBW θ, the antenna pattern is approximated as:

$$\rho(\alpha) = 1 - \frac{\alpha}{\theta}, \alpha \leq \theta. \tag{2}$$

The maximum antenna gain is achieved for the deviation angle $\alpha = 0$. To disregard the impact of side lobes, we assume efficient tapering mechanisms, such as Chebyshev tapering, with an attenuation of 60 dB [13]. A realistic antenna pattern obtained for a uniform antenna array, along with our approximation using (2), is illustrated in Fig. 2.

Additionally, we assume that the HPBW is equal for all the transmitting devices within the area of interest.

4) Received Power and Data Rate: We consider the on-body and off-body signal propagation models separately. We also assume that each user in the area may act as a blocker. The average path loss at the distance d is modeled as:

$$\text{PL}_{b/\ell/\eta}(d) = L_{b/\ell/\eta} d^{-\gamma_{b/\ell/\eta}}, \tag{3}$$

where L is the propagation constant and γ is the propagation exponent. The subscripts $b/\ell/\eta$ represent the on-body, off-body line-of-sight (LoS), and off-body non-line-of-sight (nLoS) channels, respectively.

The received power P_{rx} depends on the radio parameters and fixed position of the devices. The received power at the

Rx in our model for the case of on-body transmission can be calculated as:

$$P_{\mathrm{rx}}{=}P_{\mathrm{tx}}G_{\max}L_b d^{-\gamma_b}{=}P_{\mathrm{tx}}G_{\max}L_b(4r_b^2\sin^2\tfrac{\varphi}{2}+d_v^2)^{-\frac{\gamma_b}{2}}, \tag{4}$$

where d_v is the vertical distance between the Tx and the Rx devices, and P_{tx} is the fixed transmit power for all transmitting devices in the area of interest. For selected radio parameters and device placement on the body, the instantaneous rate during a file transfer is dictated by the Shannon–Hartley theorem as:

$$r = w\log\left(1+\min\left(\frac{P_{\mathrm{rx}}}{P_n},\mathrm{SNR}_{\max}\right)\right), \tag{5}$$

where P_n is the noise power, w is the bandwidth, and $\mathrm{SNR}_{\max}$ is the maximum SNR corresponding to the selected modulation and coding scheme (MCS). If the SNR at the Rx is greater than $\mathrm{SNR}_{\max}$, the rate r is limited to the maximum achievable data rate r_{SNR} corresponding to the selected MCS.

5) Interference: Interference at the user transferring the i-th file from the user transferring the j-th file located at the 3D distance $d_{i,j}$ for the LoS and nLoS cases is given as:

$$I_{i,j} = \begin{cases} P_{\mathrm{tx}}G_{\max}L_\ell d_{i,j}^{-\gamma_\ell}\left(1-\alpha_{i,j}\theta^{-1}\right), & \text{for LoS,} \\ P_{\mathrm{tx}}G_{\max}L_n d_{i,j}^{-\gamma_n}\left(1-\alpha_{i,j}\theta^{-1}\right), & \text{for nLoS.} \end{cases} \tag{6}$$

Interference at the user is only detected when $I_{i,j} > P_{\mathrm{thr}}$, where P_{thr} is the Rx sensitivity.

The IEEE 802.11ad/ay standards support Service Period Channel Access (SPCA), which allows multiple stations (STAs) to share the channel without introducing back-off delays. In SPCA, data exchange between STAs is scheduled using time division multiple access (TDMA). These

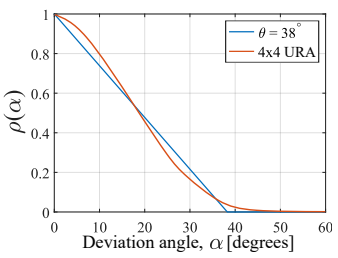

(a) Reduction factor $\rho(\alpha)$ vs. α.

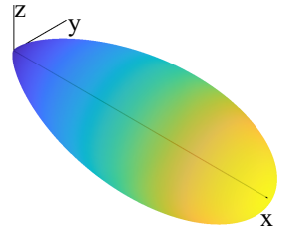

(b) Realistic pattern in 3D space.

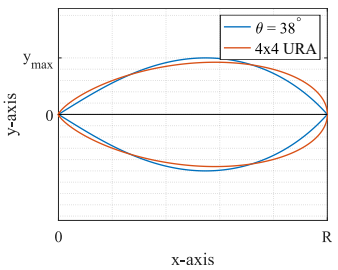

(c) 2D contour of antenna models.

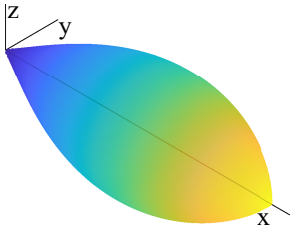

(d) Modeled pattern in 3D space.

Fig. 2: Radiation pattern for realistic antenna array and its approximation.

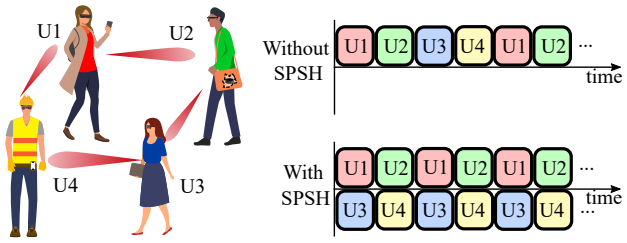

Fig. 3: SPSH abstraction.

standards also offer improvements such as clustering and spatial sharing (SPSH) to mitigate interference and enable concurrent transmissions. Clustering facilitates coordination between networks to avoid co-channel interference by scheduling transmissions in non-overlapping time slots. The SPSH allows for a further improvement in network performance by coordinating between non-interfering networks in a cluster to schedule their transmissions simultaneously.

In the context of IEEE 802.11ad/ay networks, mmWave PINs formed by the tethering of personal devices and XR headsets can be referred to as a personal basic service set (PBSS) control point (PCP) STAs and non-PCP/non-AP STAs, respectively [14]. Within a mmWave PIN, STAs can communicate directly, and if multiple PINs contend for the channel access, one of the PCPs is chosen as the Synchronizing PCP (S-PCP), which acts as the cluster head. The S-PCP then broadcasts the schedule by allowing all the listening STAs to transmit in non-overlapping periods to avoid co-channel interference.

By utilizing SPCA with SPSH, the channel can be used by several STAs simultaneously, thereby increasing the overall network capacity. An example is presented in Fig. 3, which illustrates an abstraction of SPSH. Four users need to access the channel, where each succeeding user is in the coverage area of the preceding user's PIN. In the absence of SPSH, the data of all four users is transmitted in a TDMA manner due to the direct interference they cause to each other. However, with SPSH, users 1 and 2 can transmit their data simultaneously with users 3 and 4, as they are not in direct contention for the channel. As a result, SPCA with SPSH enables more efficient utilization of the channel and improves the system performance in the crowded environments typical for XR applications.

Therefore, we assume that the neighboring active users can share the channel in a collision-free manner by employing the SPCA, and the actual data rate then depends on scheduling. If the employed clustering protocol (i.e., decentralized clustering) is efficient and leverages SPSH, some of the transmissions within a cluster can be scheduled in parallel. We consider a fair policy among the STAs to share the channel equally; hence, the actual data rate for the i-th file transmission $\tilde{r}_i$ can be approximated as:

$$\tilde{r}_i = \frac{r}{k_i+1}, \tag{7}$$

where k_i is the number of neighboring PINs sharing the channel with the user i in TDMA.

III. Performance Evaluation Methodology

In this section, we present our approach to evaluating the performance of distributed mmWave XR networks with dynamic data rates. We use a combination of queuing theory and stochastic geometry to model the system dynamics and derive expressions for the transition rate that facilitates the characterization of the stationary distribution of the system. These expressions allow us to obtain the key metrics of interest, such as the mean number of active transmissions, the mean data rate, and the mean file transmission time.

A. State Aggregation

We model the system behavior as a Markov process $X(t)$, in which every state is characterized by the number of active transmissions, user location, and locations of the user's devices. Given n ongoing file transmissions, the state of the system at time t can be defined as $X(t) = (n; \xi_1, ..., \xi_m)$, where ξ_i is the information related to the user associated with the i-th file transfer, such as the location of the user with its devices and the remaining file size.

An explicit analysis of the process $X(t)$ is complex due to its uncountable number of states. To simplify the analytical modeling, we employ the state aggregation technique to transform $X(t)$ into an aggregated birth-death process $\tilde{X}(t)$, the states of which are described by the number of active transmissions $N(t) \in [0, M]$ at any given time t. Transition rates from state n to state $n+1$ and from state n to state $n-1$ are denoted as p_n and q_n, respectively, see Fig. 4.

Importantly, the aggregated process $\tilde{X}(t)$ does not keep track of the locations of each user and device explicitly; however, the transition rates p_n and q_n are specifically designed to incorporate an estimation of network dynamics. As a result, the aggregated process allows us to obtain an approximation that reflects the averaged system behavior.

The stationary distribution, π_n, of the process follows from the corresponding birth-death formulation [15] and can be obtained as:

$$\pi_n = \pi_0 \prod_{j=1}^{n} \frac{p_{j-1}}{q_j}, \quad n = 1, ..., M, \tag{8}$$

where $\pi_0 = \left(1 + \sum_{j=1}^{M} \pi_j\right)^{-1}$. The rest of this section focuses on estimating the transition rates, p_n and q_n.

B. Transition Rates

For the aggregated process $\tilde{X}(t)$, the transition rate p_n that takes the process from state n to state $n+1$ is the arrival rate of file transfer requests within the area of interest; it is described as:

$$p_n = \lambda_R (M - n), \tag{9}$$

where λ_R is the arrival rate of file transfer requests per user and M is the total number of users.

The derivation of the transition rate q_n from state n to state $n-1$ is more complex, as it is determined not only by the number of ongoing files transfers n, but also by their transmission time T, which depends on the file size ϵ distributed exponentially with mean s, the instantaneous data rate r, and the number of neighboring PINs k. Given n active simultaneous transmissions, q_n can be expressed as:

$$q_n = \frac{n}{\mathrm{E}[T|n]} = \frac{n}{\mathrm{E}\left[\frac{\epsilon}{r}|n\right]} \approx \frac{rn}{s(\mathrm{E}\left[k|n\right]+1)}, \tag{10}$$

where $\mathrm{E}\left[k|n\right]$ is the average number of users sharing the channel. We assume that the channel is sensed by the device i as occupied if the received interference level from the neighboring device j exceeds the power threshold at the Rx, $I_{i\to j} \geq P_{\mathrm{thr}}$. This occurs when the user transmitting the i-th file is within the volume of a 3D beam of the device j. In this scenario, the user j and its k_j neighbors already utilize the channel and share it equally, which results in a reduced data rate of $\tilde{r}_j = \frac{r}{k_j+1}$. To estimate the average number of neighbors $E[k|n]$, we consider the projection of the 3D beam originating from the Tx onto the horizontal 2D plane located at the same height as the Rx, as shown in Fig. 5. We obtain the slice of the beam on the 2D horizontal plane as a conic section.

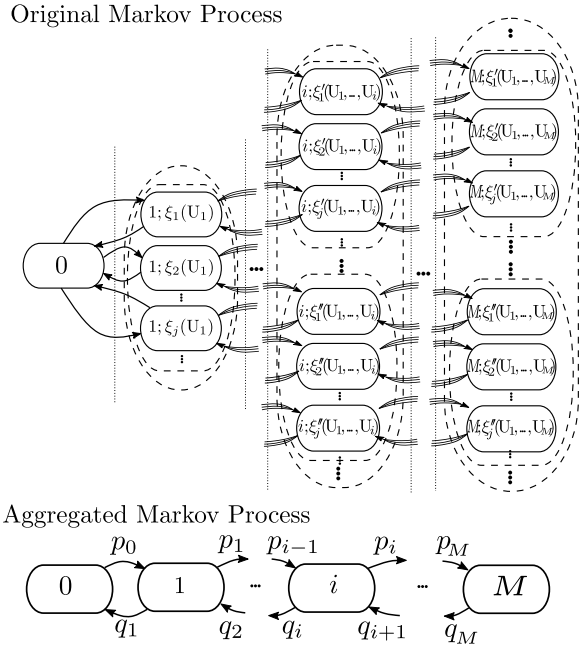

Fig. 4: Illustration of state aggregation principle.

We further calculate the semi-apex angle of the circular cone $\psi_{\ell/\eta}$ as shown in Fig. 5. The value of ψ is dependent on $R_{\ell/\eta} = \left(\frac{P_{\mathrm{tx}} G_{\max} L_{\ell/\eta}}{P_{\mathrm{thr}}}\right)^{\frac{1}{\gamma_{\ell/\eta}}}$, which represents the maximum coverage distance of the beam. Using $R_{\ell/\eta}$, we can determine the distance between the beam axis and the border of the effective beam coverage as $l_{\ell/\eta}(\alpha) = R_{\ell/\eta}\left(1 - \alpha/\theta\right)^{\frac{1}{\gamma_{\ell/\eta}}}$. We equate the distance along x-coordinate $x(\alpha) = l_{\ell/\eta}(\alpha)\cos(\alpha)$ to the fixed distance d and solve this numerically for angle $\alpha = \psi$ in LoS and nLoS cases as:

$$l_{\ell/\eta}(\psi_{\ell/\eta})\cos(\psi_{\ell/\eta}) = R_{\ell/\eta}\left(1 - \frac{\psi_{\ell/\eta}}{\theta}\right)^{\frac{1}{\gamma_{\ell/\eta}}}\cos(\psi_{\ell/\eta}) = d. \tag{11}$$

The above is a transcendental equation with respect to $\psi_{\ell/\eta}$. As a result, the sought angle $\psi_{\ell/\eta}$ at distance d for both LoS and nLoS cases can be determined numerically. Further, the

angle ϕ, which represents the angle between the horizontal plane cutting the cone and the axis of the cone, is dependent on the position of the devices. We define the angle in question as follows:

$$\phi = \arctan\left(\frac{d_v}{d_h}\right) = \arctan\left(\frac{d_v}{2r_b \sin\frac{\varphi}{2}}\right). \quad (12)$$

Proposition 1: The elliptical area on the 2D plane, $A_{\ell/\eta}$, is calculated as follows:

$$A_{\ell/\eta} = \begin{cases} \frac{\pi d_v^2 \sin(\psi_{\ell/\eta})\sin(2\psi)}{2(\sin^2(\phi) - \sin^2(\psi_{\ell/\eta}))^{\frac{3}{2}}}, & R_{\ell/\eta} > d, \\ 0, & R_{\ell/\eta} \leq d. \end{cases} \quad (13)$$

Proof. The area of the elliptical conic section is determined by the semi-minor axis [16] $a_{\ell/\eta}=\frac{d_v \sin(\psi_{\ell/\eta})}{\sqrt{\sin^2(\phi)-\sin^2(\psi_{\ell/\eta})}}$ and by the semi-major axis $b_{\ell/\eta}=\frac{d_v \sin(2\psi_{\ell/\eta})}{2(\sin^2(\phi)-\sin^2\psi_{\ell/\eta})}$. Therefore, the sought elliptical area that corresponds to the beam, within which the users may be interfered in LoS/nLoS, can be obtained as $A_{\ell/\eta} = \pi a_{\ell/\eta} b_{\ell/\eta}$. □

Note that the center of the ellipse and the axis of the oblique cone do not align; the distance between the center of the ellipse and the axis of the cone is represented as c in Fig. 5. We calculate this distance only for the LoS interference case, thus $c_\ell = b_\ell - \frac{d\sin(\psi_\ell)}{\sin(\pi-\psi_\ell-\phi)}$. To account for human body blockage of the interfering signal from other users, we utilize the exponent-based expression for the LoS probability [17] and adjust it to our system. The resulting blockage probability for the LoS beam at the state $n > 1$ may be approximated as:

$$P_b = 1 - e^{-\frac{(n-2)}{S_r}\left(2r_b\left(\frac{2}{3}(d_h+c_\ell)+\frac{4b_l}{3\pi}\right)+2{r_b}^2\right)}. \quad (14)$$

Proposition 2: An approximation for the number of users sharing the channel resources is:

$$E[k|n] = \frac{(n-1)A_\eta}{S_R} + P_b\mu_n\frac{\Gamma(n,\mu_n)}{(n-1)!}, \quad (15)$$

where $\mu_n = \frac{(n-1)(A_\ell - A_\eta)}{S_R}$, P_b is given by (14), and $\Gamma(n,\mu_n)$ is the upper incomplete gamma function.

Proof. The 2D elliptical area A_ℓ that corresponds to the area where the users may be interfered in LoS is larger than the respective area A_η for nLoS due to a substantial decrease in power received in nLoS. We observe that when a new user is located within the nLoS beam, it always senses the interference and, thus, should share the channel in TDMA. However, if it appears in the region outside of the nLoS beam and inside the LoS beam, it might share the channel, subject to being blocked by other users. For n actively transmitting users, we approximate the number of interfered users, which eventually share the channel, as follows:

$$E[k|n] = E[k_\eta|n] + E[k_\ell|n], \quad (16)$$

where $E[k_\eta|n]$ is the average number of users experiencing nLoS interference and $E[k_\ell|n]$ is the average number of users sharing the channel due to LoS interference. The average number of users under nLoS interference can be approximated due to their uniform distribution as $E[k_\eta|n] = \frac{(n-1)A_\eta}{S_R}$.

Further, the probability that m uniformly distributed users are located in the region between the borders of nLoS and LoS ellipses is given by $\frac{\mu_n^m}{m!}e^{-\mu_n}$, where $\mu_n = \frac{(n-1)(A_\ell - A_\eta)}{S_R}$ denotes the product of the area and the current density of users at the state n. The probability that i out of m users are not blocked and, therefore, are interfered by the LoS beam, can be coarsely approximated using the binomial distribution as $\binom{m}{i}P_b^{(m-i)}(1-P_b)^i$. We note that in reality, the blockage events are not independent, as several radio links can be obstructed by a single blocker. However, for the purposes of this study, the binomial distribution serves as a suitable approximation at the system level. Meanwhile, the expected number of users appearing inside the region between the borders of nLoS and LoS ellipses, subject to blockage probability P_b, can be approximated as:

$$E[k_\ell|n] = \sum_{m=1}^{n}\sum_{i=1}^{m}\frac{\mu_n^m}{m!}e^{-\mu_n} i\binom{m}{i}P_b^{(m-i)}(1-P_b)^i = P_b\mu_n\frac{\Gamma(n,\mu_n)}{(n-1)!}, \quad (17)$$

where $\Gamma(n,\mu_n)$ is the upper incomplete gamma function. □

Theorem: The stationary distribution of the process $\tilde{X}(t)$ can be approximated as:

$$\pi_n = \frac{\pi_0 M!}{n!(M-n)!}\left(\frac{s\lambda_R}{r}\right)^n \prod_{j=1}^{n}\left(\frac{(j-1)A_\eta}{S_R} + P_b\mu_j\frac{\Gamma(j,\mu_j)}{(j-1)!} + 1\right), \quad (18)$$

where $\mu_j = \frac{(j-1)(A_\ell - A_\eta)}{S_R}$, P_b is given by (14) and $\Gamma(j,\mu_j)$ is the upper incomplete gamma function.

Proof. By substituting into (8) the expressions for p_n and q_n given by (9) and (18), respectively, we obtain the intended result. □

With the above stationary distribution, we establish the relevant system-level metrics such as the mean number of users simultaneously transferring files $E[N]$, the mean data rate $E[\tilde{r}]$, and the mean file transmission duration $E[T]$:

$$E[N] = \sum_{n=1}^{M} n\pi_n, E[\tilde{r}] = \sum_{n=1}^{M}\frac{r\pi_n}{E[k|n]+1}, E[T] = \frac{E[N]}{\sum_{n=0}^{M}(M-n)\lambda_R\pi_n}. \quad (19)$$

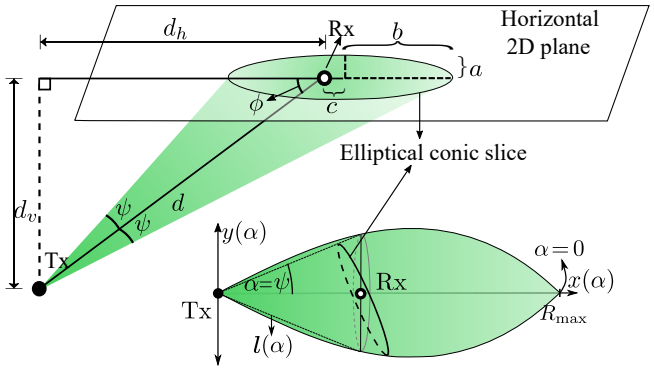

Fig. 5: Elliptical projection of 3D beam onto 2D plane and related parameters.

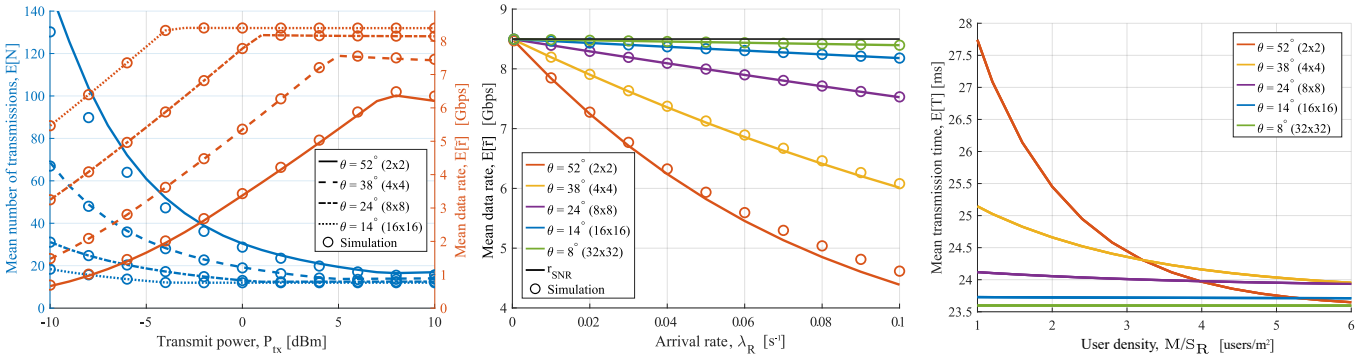

(a) Mean number of transmissions and mean data rate vs. transmit power.

(b) Mean data rate vs. arrival rate.

(c) E[T] vs. user density.

Fig. 6: Impact of small-scale movement and beam misalignment during on-body communication on system performance.

TABLE I: System parameters

Parameter	Notation	Value
Area of interest	S_R	100 m^2
Number of users	M	200
Mean human blocker height	h_b	1.8 m
Mean human blocker radius	r_b	0.15 m
Height of Rx	r_{R}	1.75 m
Height of Tx	r_{T}	0.9 m
Central angle	φ	60°
Carrier frequency	f	60 GHz
Carrier bandwidth	w	2.16 GHz
Mean file size	δ	20 MB
Receiver sensitivity	P_{thr}	-78 dBm
Transmit power	P_{tx}	10 dBm
Noise figure	NF	9 dB
Power spectral density of noise	N_0	174 dBm/Hz
Maximum SNR [18]	$\mathrm{SNR}_{\mathrm{max}}$	17 dB (MCS 17)

IV. Numerical Results

In this section, we present our numerical results to illustrate the impact of various parameters. We consider an environment where each user is equipped with an XR headset and an accompanying personal device, which are wirelessly paired to each other via direct mmWave links using IEEE 802.11ay radio technology. The personal device sends the rendered data to the XR headset, and we consider its size to be exponentially distributed with the mean of s, which we refer to as a file. To validate our analytical results, we perform Monte Carlo simulations using Matlab. For these, the height and width of users are assumed to follow a Gaussian distribution, which leads to a variable distance between devices. The height of the users has a standard deviation of 0.05, while the radius of the users has a standard deviation of 0.01.

In our model, we differentiate between on-body propagation, LoS off-body propagation, and nLoS off-body propagation. We employ several channel propagation models, which we adapt to the $PL(d) = Ld^{-\gamma}$ pathloss format. For on-body propagation, we use $L_{\mathrm{B}} = 71.2$ and $\gamma_{\mathrm{B}} = 4.1$ [19]. For LoS off-body propagation, we use L_ℓ = 68.15 and γ_ℓ = 1.88 [20], while for nLoS off-body propagation, a 30 dB penalty is applied to the link budget when a beam is blocked by a human body [21]. We evaluate the impact of different antenna radiation patterns with varying numbers of antenna elements by utilizing Matlab's Sensor Array Analyzer for uniform rectangular arrays (URAs) of 2x2, 4x4, 8x8, and 16x16 elements.

To reduce the sidelobes and focus the transmit energy within the main lobe, we apply a 60 dB Chebyshev taper to all our antenna models in simulation. In our analytical results, we approximate the shape of the main lobes by using the pattern obtained using (2) with the corresponding HPBW angle θ. In the proposed analysis, we employ a cascade of approximations, which includes antenna abstraction, state aggregation, and approximation for the number of users sharing the channel resources in a TDMA manner. We validate selected analytical results by comparing them with simulation output to demonstrate the tightness of our analytical approximations for the parameters of interest. The rest of the system parameters utilized throughout this section are summarized in Table I.

In Fig. 6a, we evaluate the impact of transmit power on the mean number of simultaneous file transmissions and the mean data rate for different numbers of antenna elements. The number of simultaneous transmissions decreases with higher transmit power and with an increase in the number of antenna elements. Additionally, the data rate grows for a higher transmit power and a larger number of antenna elements in an antenna array. The data rate saturates when the instantaneous rate approaches r_{SNR}. Since for wider beams (fewer antenna elements), more users are sharing the channel, the effective data rate is lower as compared to that for antennas with a higher number of elements that yield smaller coverage areas. The number of simultaneous transmissions decreases drastically for antennas with fewer elements, while for antennas with more antenna elements, the number of transmissions saturates. Antennas with a higher number of elements perform better in terms of data rate than antennas with fewer elements due to higher received power and smaller interference footprints. If power control [22] and beamwidth control [23] algorithms at the MAC layer of IEEE 802.11ay are additionally applied, the performance of distributed networks such as wearable PINs can be significantly improved while also enhancing their energy efficiency.

In Fig. 6b, we examine the impact of the increased arrival rate of transmission requests per a unit area on the mean data rate for different numbers of antenna elements. It can be observed that the mean data rate decreases as the arrival rate grows and the effect of a higher arrival rate is more pronounced for antennas with fewer elements. This is because a larger coverage area enables users to share the channel resources more frequently, thereby ultimately reducing the mean data rate. Here, antennas with more antenna elements have a lower impact on the system performance, as then PINs have comparatively fewer users sharing the channel resources due to a smaller coverage area. We also note that the analytical results align tightly with the simulation output for the parameters of interest despite our cascade of approximations.

Finally, in Fig. 6c, we present the impact of blocker (user) density on the mean transmission time for different numbers of antenna elements. Our analytical results indicate that antennas with fewer antenna elements benefit the most from a higher blocker density, which improves the chances of occlusion, thereby preventing the interfering signals from reaching other users and providing spatial isolation from interference. For narrower beams (more antenna elements), the blockage effect becomes less prominent due to a smaller interference footprint.

V. Conclusion

In this paper, we investigate the system-level performance of wearable PINs that utilize 3D directional mmWave beams with adaptive data rates in an environment subjected to the presence of human blockers. We provide a tight analytical approximation that allows studying various XR system trade-offs associated with the averaged performance indicators, such as the number of active users, data rate, and transmission time.

We observe that increased numbers of antenna elements and transmit powers lead to enhanced performance. The use of a higher number of antenna elements has a lower impact on the performance in scenarios with high arrival rates and frequent blockages, while fewer antenna elements yield more noticeable performance effects.

In addition, increasing the transmit power beyond a certain threshold does not lead to further improvements in performance, which means that the energy efficiency of the system at hand may be enhanced by employing appropriate power control schemes and by utilizing a larger number of antenna elements. Finally, we note that wearable PINs may display better performance in the presence of more blockers, as these offer improved spatial isolation.

Acknowledgments

This work was supported by the European Union's Horizon 2020 Research and Innovation programme under the Marie Skłodowska-Curie grant agreement No. 813278 (A-WEAR; http://www.a-wear.eu/). This work was also supported by the Academy of Finland (projects RADIANT, IDEA-MILL, and SOLID).

References

[1] 3GPP TSG SA TR 26.806, "Study on Tethering AR Glasses – Architectures, QoS and Media Aspects (Release 18)," 2023.

[2] 3GPP TSG SA TR 26.859, "Study on Personal Internet of Things (PIoT) networks (Release 18)," 2022.

[3] 3GPP TSG SA TR 22.856, "Feasibility Study on Localized Mobile Metaverse Services (Release 19)," 2023.

[4] 3GPP TSG RAN TR 38.838, "Study on XR (Extended Reality) Evaluations for NR (Release 18)," 2022.

[5] K. Venugopal, M. C. Valenti, and R. W. Heath, "Device-to-Device Millimeter Wave Communications: Interference, Coverage, Rate, and Finite Topologies," *IEEE Transactions on Wireless Communications*, vol. 15, no. 9, pp. 6175–6188, 2016.

[6] G. George, K. Venugopal, A. Lozano, and R. W. Heath, "Enclosed mmWave Wearable Networks: Feasibility and Performance," *IEEE Transactions on Wireless Communications*, vol. 16, no. 4, pp. 2300–2313, 2017.

[7] M. N. Anjum, H. Wang, and H. Fang, "Prospects of 60 GHz mmWave WBAN: A PHY-MAC Joint Approach," *IEEE Transactions on Vehicular Technology*, vol. 69, no. 6, pp. 6153–6164, 2020.

[8] Y. Wang and G. de Veciana, "Dense Indoor mmWave Wearable Networks: Managing Interference and Scalable MAC," in *14th International Symposium on Modeling and Optimization in Mobile, Ad Hoc, and Wireless Networks (WiOpt)*, pp. 1–8, 2016.

[9] V. Begishev, E. Sopin, D. Moltchanov, R. Pirmagomedov, A. Samuylov, S. Andreev, Y. Koucheryavy, and K. Samouylov, "Performance Analysis of Multi-Band Microwave and Millimeter-Wave Operation in 5G NR Systems," *IEEE Transactions on Wireless Communications*, vol. 20, no. 6, pp. 3475–3490, 2021.

[10] R. Fantacci and B. Picano, "End-to-End Delay Bound for Wireless uVR Services over 6G Terahertz Communications," *IEEE Internet of Things Journal*, vol. 8, no. 23, pp. 17090–17099, 2021.

[11] A. Ali, O. Galinina, J. Hosek, and S. Andreev, "Performance Evaluation of Dynamic Computation Offloading Capability for Industrial Wearables," in *IEEE 32nd Annual International Symposium on Personal, Indoor and Mobile Radio Communications (PIMRC)*, pp. 1–7, 2021.

[12] J. K. Sundararajan, H.-J. Kwon, O. Awoniyi-Oteri, Y. Kim, C.-P. Li, J. Damnjanovic, S. Zhou, R. Ma, Y. Tokgoz, P. Hande, T. Luo, K. Mukkavilli, and T. Ji, "Performance Evaluation of Extended Reality Applications in 5G NR System," in *IEEE 32nd Annual International Symposium on Personal, Indoor and Mobile Radio Communications (PIMRC)*, pp. 1–7, 2021.

[13] R. Haupt, "Reducing Grating Lobes due to Subarray Amplitude Tapering," *IEEE Transactions on Antennas and Propagation*, vol. 33, no. 8, pp. 846–850, 1985.

[14] Q. Chen, X. Peng, J. Yang, and F. Chin, "Spatial Reuse Strategy in mmWave WPANs with Directional Antennas," in *IEEE Global Communications Conference (GLOBECOM)*, pp. 5392–5397, 2012.

[15] L. Kleinrock, *Queueing Systems: Theory*. John Wiley, 1975.

[16] H. C. Rajpoot, "Analysis of Oblique Frustum of a Right Circular Cone," *International Journal of Mathematics and Physical Sciences Research*, vol. 2, pp. 1–17, 2015.

[17] K. Venugopal, M. C. Valenti, and R. W. Heath, "Analysis of Millimeter Wave Networked Wearables in Crowded Environments," in *49th Asilomar Conference on Signals, Systems and Computers*, pp. 872–876, 2015.

[18] C. R. C. M. da Silva, A. Lomayev, C. Chen, and C. Cordeiro, "Analysis and Simulation of the IEEE 802.11ay Single-Carrier PHY," in *IEEE International Conference on Communications (ICC)*, pp. 1–6, 2018.

[19] R. Aminzadeh, A. Thielens, M. Zhadobov, L. Martens, and W. Joseph, "WBAN Channel Modeling for 900 MHz and 60 GHz Communications," *IEEE Transactions on Antennas and Propagation*, vol. 69, no. 7, pp. 4083–4092, 2020.

[20] A. Al-Hourani, S. Chandrasekharan, and S. Kandeepan, "Path Loss Study for Millimeter Wave Device-to-Device Communications in Urban Environment," in *IEEE International Conference on Communications Workshops (ICC)*, pp. 102–107, 2014.

[21] B. Li, Z. Zhou, W. Zouebin, and G. Du, "On the Efficient Beam-Forming Training for 60GHz Wireless Personal Area Networks," *IEEE Transactions on Wireless Communications*, vol. 12, pp. 504–515, 2013.

[22] C. Chen, O. Kedem, C. R. C. M. da Silva, and C. Cordeiro, "Millimeter-Wave Fixed Wireless Access Using IEEE 802.11ay," *IEEE Communications Magazine*, vol. 57, no. 12, pp. 98–104, 2019.

[23] H. Chung, J. Kang, H. Kim, Y. M. Park, and S. Kim, "Adaptive Beamwidth Control for mmWave Beam Tracking," *IEEE Communications Letters*, vol. 25, no. 1, pp. 137–141, 2021.